49th AIAA Aerospace Sciences Meeting including the New Horizons Forum and Aerospace Exposition
4 - 7 January 2011, Orlando, Florida
AIAA 2011-553

Design and Analysis of a Bio-Inspired Warping Tail for MAV Applications

Zach Votaw[1], Zach Gaston[2], Aron Brezina[3], Asela Benthara[4], Haibo Dong[5]
Department of Mechanical & Materials Engineering
Wright State University
Dayton, OH 45435

This paper examines a unique method of flight control for flapping wing micro air vehicles. Instead of employing rigid body joints and flaps for torsional agility, the technique implemented a compliant tail mechanism. The bio-inspired technique utilizes a flexible carbon fiber (CF) tail to mimic body posture changes of insects, specifically lateral abdomen deflections. This method of flight control was examined using Flytech's WowWee Dragonfly as an experimental platform. Trajectory analysis was done to generate a three dimensional flight path of the vehicle for examining flight characteristics. ANSYS FLUENT fluid dynamics software with GAMBIT and Solidworks CAD software were utilized to investigate aerodynamic torques and gravitational torques corresponding to active tail warping. The results provided evidences suggesting that the warping tail administered adequate control authority for basic maneuvering.

Nomenclature

α_t	=	angle of attack of the tail
CF	=	carbon fiber
CFD	=	computational fluid dynamics
CG	=	center of gravity
λ	=	pitch angle
L'_g	=	roll moment due to gravitational torque
M	=	magnification
MAV	=	micro air vehicle
Re	=	Reynolds number
θ_t	=	tail set-angle relative to wing root
X	=	longitudinal axis
Y	=	lateral axis
Z	=	directional axis

I. Introduction

IT is no secret that winged insects are masters of flying in unpredictable and constrained environments. Their aerobatics at low Reynolds numbers (Re) and agile flight undoubtedly exceeds anything made by man. Therefore, examining the mechanics of insect flight is a valuable practice for micro air vehicle (MAV) design. In fact, great efforts in the design of MAVs are being expended on mimicking the natural flight of insects. Although the mechanics of insect flight are still by and large in the descriptive stage, extensive research shows that wing kinematics are the primary means of flight control. Kinematic parameters such as phase relationships, stroke plane

[1] Undergraduate Student, AIAA Student Member, Votaw.3@wright.edu
[2] Undergraduate Student, AIAA Student Member
[3] Undergraduate Student, AIAA Student Member, Brezina.2@wright.edu
[4] Graduate Student, AIAA Student Member
[5] Assistant Professor, AIAA Senior Member

angle, stroke plane amplitude, wing beat frequency, and wing rotation all play significant roles in flight speed and trajectory.[1-4] However, it has also been suggested through considerable tethered flight analysis, that body posture plays a role in insect flight control as well.[5-10] Tethered flights from the Drosophila melanogaster (fruit fly) subjected to visual stimuli and Schistocerca greggaria (desert locust) subjected to wind modulation has provided evidence indicating that changes in body posture, such as deflections of abdomen and appendages, are used for aerodynamic torques and gravitational torques. These insects used lateral abdominal deflections aerodynamically for rudder steering[7,8] and gravitationally for roll maneuvering.[9] Further research shows insects used dorsoventral abdominal deflections to induce pitching torques.[10] In light of these studies, it seems reasonable to investigate the accommodation of these techniques (postural changes) in the development of flight control for flapping wing MAVs.

The bulk of conventional fixed wing MAV's and flapping wing MAVs that have been developed (e.g. DelflyII,[11] Micro Bat[12]) utilize rigid body joints such as rudder and elevator control flaps for torsional agility (yaw, roll, and pitch). Rigid body joints implementing blatant control surfaces, although a functional strategy for flight control, are not found in nature and deviate from the "hide in plain sight" mission attribute. While many efforts are being made to eliminate the need for control surfaces with the solitary use of wing kinematics, there may be unique advantages in utilizing both in combination. It is believed that body surface kinematics could provide the MAV with additional control authority for executing advanced maneuvers and provide a means for trimming the vehicle or maintaining stability in gusty environments. Employing a warping tail, as inspired by how flying insects use body posture, is an intriguing approach for achieving bio-inspired flight control.

This approach to bio-inspired flight control is similar in character (but different in function) to the University of Florida's flexible wing methodology. The researchers at the University of Florida have developed an impressive fleet of MAVs that utilize composite materials to make up adaptive wing structures.[13-16] These adaptive wings were demonstrated to enable sufficient maneuverability and also alleviate environmental disturbances.[13] The utilization of adaptive wings have been under investigation by a variety of researchers for years and have a long history in aviation.[17] Nevertheless, very little has been done in applying these flexible wing concepts to tail and rudder mechanisms. Therefore a large portion of this work is devoted to establishing a framework of simple design, manufacturing, and testing methodologies for warping tail implementation on a flapping wing MAV. The work presented in this paper is the first step towards developing a flapping wing MAV that uses a warping tail mechanism, inspired by the body kinematics of insects, as a means for flight control.

II. Methodology

A. Test Vehicle

To investigate the viability of a warping tail mechanism, an experimental vehicle was required. The FlyTech WowWee Dragonfly (Fig. 1) was a suitable testing platform because it was modifiable, readily available, economical, and proved to be an effective flapping wing vehicle. The WowWee Dragonfly resembled a biplane model that used the clap and peel technique to generate lift and thrust much like the Delfly I.[11] It incorporated a lightweight foam body that resembled a dragonfly, a flat tail that served as a horizontal stabilizer, and a propeller at the rear for directional control. Significant modifications were made to convert it into suitable platform for tail testing. The foam casing, appendages, receiver, and tail with rear propeller were removed, leaving the actuator, fuselage, and wings as the test bed. A Plantraco Micro-9-S Servo Receiver (1.1g) with micro JST connectors replaced the original receiver in order to make battery and servo transactions manageable. Also, a Blue Arrow S0251 Ultra Micro Servo (2.5g) was used to actuate the tail for steering. Lastly, a Full River fifty milliamp hour LiPo battery (1.72g) supplied the power.

Figure 1. FlyTech WowWee Dragonfly

B. Pivoting Tail

The torsional effects of a laterally deflecting tail were first gauged using a pivoting conventional tail shown in Fig. 2. Instead of using flaps on a vertical fin for rudder steering, the conventional tail was fixed to the end of a pivoting arm. The pivoting arm was a CF rod 165.1mm in length and 1mm in diameter which was joined to a servo arm. A bracket was fabricated (Fig. 3) to secure the servo and tail assembly to the fuselage of the experimental

vehicle. The servo laterally rotated the rigid tail 45° from center position to initiate aerodynamic and gravitational torques. Because lateral tail deflections were the primary focus of this study, an elevator mechanism was not incorporated into the experimental vehicle for longitudinal controls. The angle of the tail relative to the wing root was positioned to provide pitch stability and longitudinal control was simply achieved by varying the flapping frequency. After examining the control influence of the pivoting conventional tail, further investigation was done for the development of a flexible tail.

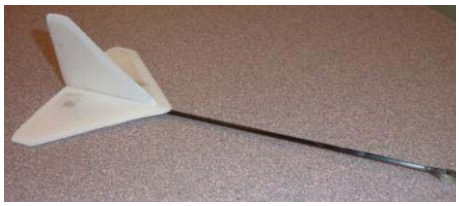

Figure 2. Pivoting Foam T-Tail

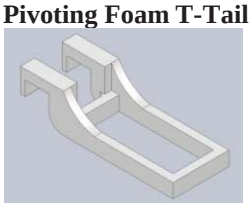

Figure 3. Servo Bracket

C. Warping Tail

Many considerations were taken in the development of an actively controlled flexible tail. In an effort to enhance the bio-inspired qualities of the experimental vehicle, the shape and length of the tail's vertical component was designed to resemble the profile of a dragonfly's abdomen. A horizontal stabilizer (HS) was oriented on top of the vertical element in the T-tail configuration in effort to keep it out of the wake of the wings. Appropriate HS sizes and tail set-angles θ_t had to be distinguished through trial and error to provide a suitable range for pitch stability. The θ_t which provided the best pitch stability ranged from 10° to 30° relative to the wing root (top edge of the airframe) as shown in Fig. 4. The θ_t was required to keep the pitch angle λ positive for sufficient lift generation. Two brackets were constructed accordingly; one which positioned the tail at θ_t=10° and the other at θ_t =30°. Both were used and compared in flight observation and trajectory analysis. The warping tail was tethered to a servo arm which actuated the tail through a linkage system. The final parameters of the experimental vehicle are presented in Table. 1.

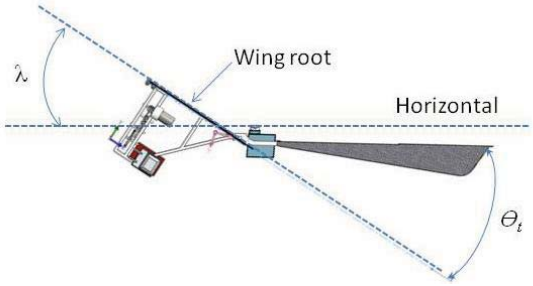

Figure 4. Vehicle Orientation during Steady Flight

Table 1. Parameters of Test Vehicle

Parameter	*Parameter Value*
Vehicle Mass	20.55 g
Flapping Frequency	9-11 Hz
Wing Span	406.4 mm
Wing Area	17322.4 mm^2
Mean Chord length	82.5 mm
Body length	285 mm
Tail Mass	1.89 g

CF composite materials were the most favorable medium for fabrication. CF composites provide flexibility without jeopardizing durability, are generally workable, and have proved to be an effective material for adaptable mechanisms such as the University of Florida's morphing wing.[11,15] 3K CF tow was used for the skeletal structure of the tail which was embedded into multiple layers of CF tissue and infused with laminating epoxy. The CF tissue had a random fiber orientation which allowed for uniform elastic properties. The tail stiffness was primarily dependant on the amount of CF tissue layers used and the gauge of the CF tow embedded in the tissue. A detailed description of the construction process is explained here.

1. A tail design is drawn using CAD software to serve as a template for the arrangement of CF tow and is placed on flat plate that can fit into a vacuum seal bag.
2. Transparent polyester film is placed over the drawing and secured tightly to the flat plate with tape. This is shown on the left of Fig. 5.
3. Pro-set 135 resin and Pro-set 224 hardener are mixed according to manufacturer specifications for laminating epoxy using an electronic bench scale to measure the mass ratio. This is shown in the center of Fig. 5.
4. 3K CF tow is coated with epoxy and manually placed on the polyester film using the drawing as a template. This is seen in the right of Fig. 5.
5. The CF tow is left to cure for 8 hours.

Figure 5. Tail Construction Procedure.

6. The cured skeletal structure is carefully removed from the polyester film, and another mixture of laminating epoxy is spread uniformly onto the transparent film using a paint brush and spreading tool. This is shown in the left of Fig. 6.
7. A layer of CF tissue is placed on top of the spread epoxy and gently pressed.
8. A thin uniform coating of laminating epoxy is applied on top of the CF tissue and another layer of CF tissue is placed. This is seen in the center of Fig. 6. Multiple layers can be added to increase stiffness.
9. The CF skeletal structure is placed on the CF tissue and additional epoxy and CF tissue layers are applied on top of it in the same manner as before. This is shown in the right of Fig. 6.

Figure 6. Tail Construction Procedure.

10. Another sheet of polyester film is placed on top the CF laminates to prevent the resin from adhering to the vacuum bag (Left Fig. 7).
11. The assembly is placed into a vacuum bag and subsequently vacuum sealed (Center Fig. 7).
12. The tail is left to cure for 12 hours at room temperature.
13. The components are removed from the bag and cut out.
14. Two custom control horns are joined, with epoxy, to one side of the vertical fin leaving the top surface of the horn slightly elevated above the top edge of the fin.
15. After curing, two additional control horns are joined symmetrically, in the same fashion, on the other side of the vertical fin.
16. The horizontal fin is joined with epoxy to the top surface of the rear elevated control horn.
17. The tail is fixed to the custom servo bracket and the linkage system is installed. The finished composite tail is shown on the right in Fig. 7.

Figure 7. Tail Construction Procedure.

The warping tail approach to flight control was examined using three simple methods. Trajectory analysis was used to generate a three dimensional flight path of the vehicle for documentation and close examination of the vehicle's flight characteristics. Solidworks CAD software was used to investigate the gravitational torque generated by lateral tail deflection and ANSYS FLUENT computational fluid dynamics (CFD) software was used to investigate aerodynamic torques due to lateral tail deflection. The Solidworks modeling and CFD analysis were performed primarily to validate the results gathered from free flight observations and trajectory analysis.

D. Trajectory Analysis

Tracking the flight path of the vehicle was valuable for close examination of the warping tail's flight performance. Parameters such as velocity, turning radius, turning duration, wing beats per turn, and general flight behavior were easily documented and compared with results from other warping tail models. Videos were obtained using two Sony Handycam HDR-CX550V Camcorders which are capable of shooting footage in 1080i. With both cameras placed in an equidistant relationship, orthogonal to one another, settings were made identical on both cameras such as video quality and optical/digital zoom. The cameras were synchronized and videos of the flying MAV were obtained so that turning duration and radius could be measured. From these videos, the open-source video encoding tool, FFMPEG, was used to sample the video sequences at 30 frames per second, which is the native recording rate of the camcorder. Because the flying speed of the MAV is relatively low in comparison to the sampling rate, it was determined that this sampling frequency was sufficient to prevent aliasing of the data. These image sequences were used to create two orthographic perspective projections of the MAV's flight pattern over time. The projection data was analyzed by taking the captured still images and converting the data from image space (pixel) coordinates to real global coordinates. The images were corrected using an application of the camera correction matrix that is composed of skew factors and lens distortion parameters that are gathered using an open source computer vision package called OpenCV. This process has been used in previous work by Dong et al.[18] The fully corrected images are then read into image processing software.

Previously, point tracking was performed using commercial animation software such as Autodesk Maya. Because licenses for those softwares are expensive and the software has many unused features that require a great deal of system resources, new efforts were made to provide a simple, uniform platform for processing high speed data. The in-house point tracking code was developed using the MATLAB computing language with the Image Processing Toolbox installed to read in a series of images from multiple cameras to capture the pixel coordinates of rigid bodies in the images. The current version of software is a manual tracking mode, where each still image is displayed and a desired point in the frame is selected manually by the user. This data is stored from both the x-z plane and the y-z plane in pixel coordinates. With a known size and shape of the rigid object, pixel coordinates are transformed into real space coordinates using the Eq. (1) shown below.

$$\begin{bmatrix} x \\ y \\ z \end{bmatrix}_{real} = M \begin{bmatrix} x \\ y \\ z \end{bmatrix}_{pixel} \tag{1}$$

In this equation, M is the magnification factor of the camera lens. The raw data that is sampled from the image sequences is filtered using a 6^{th} order Buttersworth filter, to alleviate some of the user input errors and minor outliers generated from using this reconstruction and tracking process. A simple MATLAB plotting script was used to visualize the real space coordinates of the flying MAV in both 3D space and an overhead, x-y plane, projection.

E. Center of Gravity Displacement Analysis

The warping tail design was primarily expected to act as a rudder for directional control. However, large tail deflections were also expected to displace the vehicles CG. A significant shift in the aircraft's CG would subsequently initiate a gravitational torque L'_g causing the vehicle to roll. A mild roll maneuver was anticipated to supplement the aircraft's turning abilities by minimizing turning radius and sideslip. In order to gauge the warping tail's influence on CG displacement, a simple static experiment was performed. The vehicle was tethered to the ceiling with two strings along its longitudinal axis and the wingspan was stabilized horizontally. As the tail was deflected, the vehicle promptly responded with a roll in the same direction. As the tail was deflected in the opposite direction, the vehicle rolled promptly to the other side. These results gave evidence to suggest that lateral tail deflection contributed enough gravitational torque to influence roll. A measurement of L'_g generated about the longitudinal axis was calculated quantitatively by using the mass properties evaluation tool in Solidworks. Each component of the experimental vehicle was drawn in Solidworks according to dimension and assigned its measured mass value. After two assembly models were completed, one encompassing 0^o lateral tail deflection and the other

encompassing 60° lateral tail deflection, a common coordinate system was established at the front of the vehicle as shown in Fig. 8. The X direction along the airframe represented the longitudinal axis, the Y direction along the wingspan represented lateral axis, and the Z direction aimed upward represented the directional axis. Since the rolling moment was being investigated, the displacement of CG in the Y direction was of most interest.

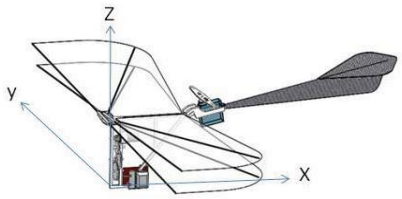

Figure 8. Coordinate System for CG Location

F. Computational Fluid Dynamics Analysis

The purpose of simulating the computational analysis was to get a numerical estimate for the drag and lift forces acting on the warping tail and the subsequent moments exerted on the aircraft. The numerical estimates were expected to verify and explain the flight characteristics observed from the trajectory analysis and free flight testing. The inlet velocity was set at 2.5 m/s and was determined by examining the average ground velocity of the vehicle flown indoors from the trajectory analysis. Two cases were ran, each administering different angles of attack; α_t = -10° for the first case and α_t = -30° for the second. These angles were derived after examining the direction of air flow generated by the wings over the tail. The direction of airflow from the wings was considered to be parallel to the wing root. The angle α_t corresponded to θ_t, which was governed by the two brackets made for the tail set-angle.

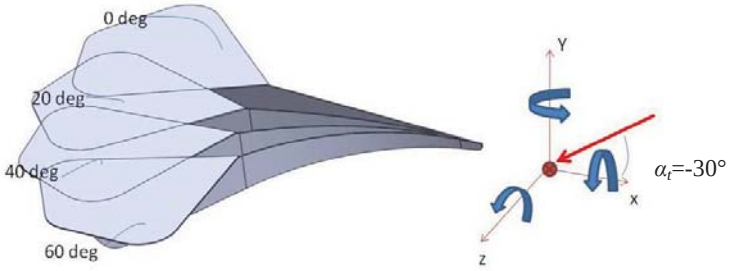

Figure 9. Tail Deflection Angles. *Also shown are the positive values of the moments and the angle of the incoming flow α_t.*

The warping tail was modeled as a rigid structure. Solidworks was used to design the basic geometries shown in Fig. 9. Four deflection angles of 0°, 20°, 40°, and 60° were modeled in the simulation and maximum deflection of 60° was measured from the actual tail motion of the experimental MAV. The Solidworks model was then transferred to GAMBIT which was used for meshing and assigning boundaries. Tetra hybrid elements were used for the meshing and dimensions for the far field, inlet, and outlet were assigned as shown in the Fig. 10. The mesh was exported into FLUENT for making the CFD computational simulation. After the mesh refinements in FLUENT, the number of mesh elements present in each simulation were close to 10^4.

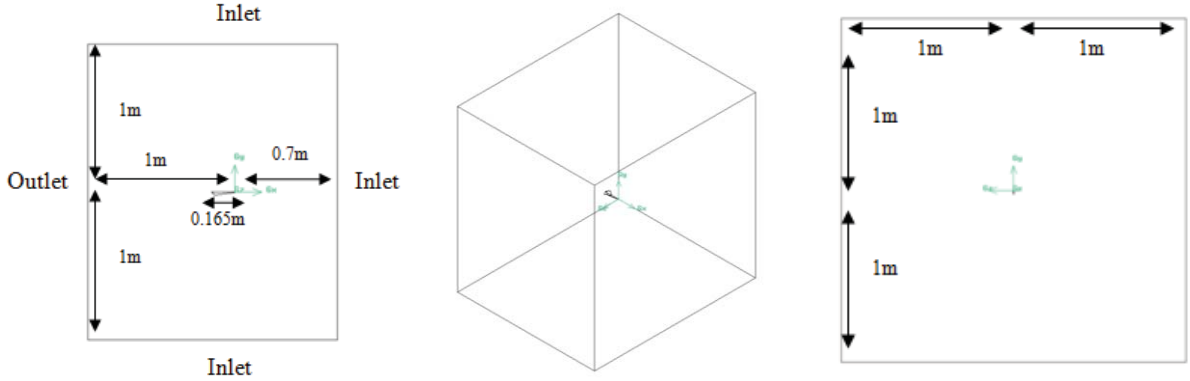

Figure 10. Far Field Dimensions. *Side view (left), isometric view (center), front view (right).*

For the solution method in FLUENT, a SIMPLE scheme was used in which the moment equation was discritized using second order upwind scheme. The Reynolds number was approximately 1700 for the simulations. A laminar viscous model was used when simulating the flow conditions. It was noted that under real conditions the warping tail experienced unsteady air flow due to wake affects of the flapping wings. However, understanding the turbulent flow from the wings encountered by the flexible tail was beyond the scope of this study.

III. Results

A. Trajectory Analysis

Two flights paths were recorded of the MAV with the tail positioned at θ_t =10° (tail 1) and θ_t= 30° (tail 2). Each flight was made by the same pilot using the same power source for each flight. The MAV was flown in the same environment and all data was obtained on the same day under the same setup conditions. To minimize the discrepancies in pilot flight control inputs, the pilot made efforts to bring the MAV to the same relative altitude, in stable flight, before entering a spiral pattern at full throttle. Once reaching the same relative altitude at the bottom of the spiral, the pilot then returned the MAV to a stable flight path. Table 2 summarizes the data obtained from two separate flights involving two different tails.

From Test 1, the global coordinates were obtained from the flight where a controlled, downward spiral was performed and the median 180 degree yaw turn was selected for analysis. This specific turn as well as the global coordinates of the recorded flight is shown in Fig. 11. From this specified turn, the duration of the turn, turning radius, and velocity profile were measured. From the duration of time to complete the 180 degree turn and the known wing beat rate of the MAV, the beats per turn were calculated and included with the previously shown table.

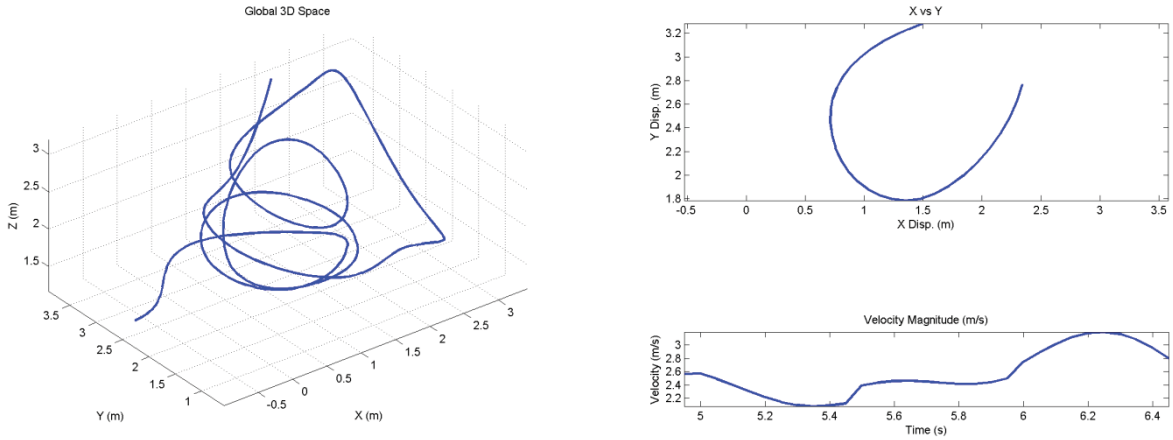

Figure 11. Tail 1 Point Tracking. *Global coordinates of entire flight (left), isolated 180 degree turn (right top), and velocity magnitude for turn (right bottom)*

The subsequent flight, Test 2, was analyzed in the same manner as before. The plot of the MAV trajectory is shown in Fig. 12 and the calculated turning radius, duration, and beats per turn are included in the previously shown table.

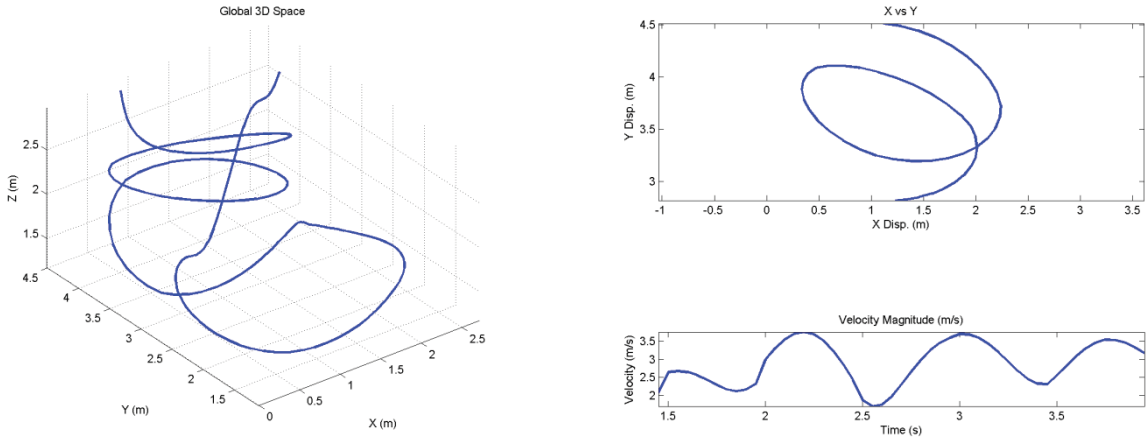

Figure 12. Tail 2 Point Tracking. *Global coordinates of entire flight (left), isolated 180 degree turn (right top), and velocity magnitude for turn (right bottom).*

Table 2. Summary of Turning Radius and Duration from Various Tests

	Tail 1 ($\theta_t=10^o$)	*Tail 2* ($\theta_t=30^o$)
Turning Radius (m)	0.6630	0.3858
Duration of Turn (s)	0.9997	0.7503
Beats per Turn	9.613	7.214

B. Center of Gravity Analysis

The mass properties analysis tool indicated that a maximum tail deflection of 60^o displaced the CG 7.19mm from the X-axis in the direction of the tail deflection. These results are shown Table 3 and Fig. 13. The pink indicator marks the position of model's CG. The displacement resulted in a rolling moment L'_g of 1449.47 (10^{-6} Nm) which was computed by multiplying the gravitational force on the vehicle and Y coordinate value. The CG analysis provided firm quantitative evidence to show that lateral tail deflection indeed generated roll torques to influence roll motion of the vehicle.

Table 3. Center of Gravity Analysis Results

	Tail at 0 degree deflection	*Tail at 60 degree deflection*
Mass (g)	20.55	20.55
X displacement (mm)	55.99	52.89
Y displacement (mm)	-0.69	-7.19
Z displacement (mm)	43.65	43.10
Rolling Moment L'_g (Nm)	$139.1_* 10^{-6}$ Nm	$1449.5_* 10^{-6}$

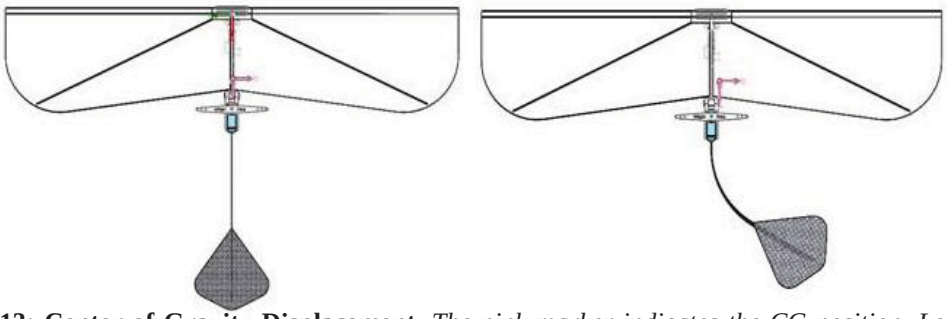

Figure 13: Center of Gravity Displacement. *The pink marker indicates the CG position. Left image shows assembly model of tail with zero deflection. Right image shows assembly model of tail with 60^o deflection.*

C. Computational Fluid Dynamics Results

The CFD analysis on the warping tail provided insight as to what aerodynamic moments were being generated on the vehicle during flight. The CFD analysis was performed primarily to validate observations gathered from free flight testing and trajectory analysis. The drag and lift forces generated on the tail for four different degrees of deflection are displayed in Table 4 and Table 5 along with the resulting moments contributed by each about the vehicles CG. Table 4 and Table 5 show the results from tail 1 and tail 2 respectively. Also, Fig. 14 and Fig. 15 indicate the pressure distributions over the top and incurved surface of tail 1 and tail 2 respectively.

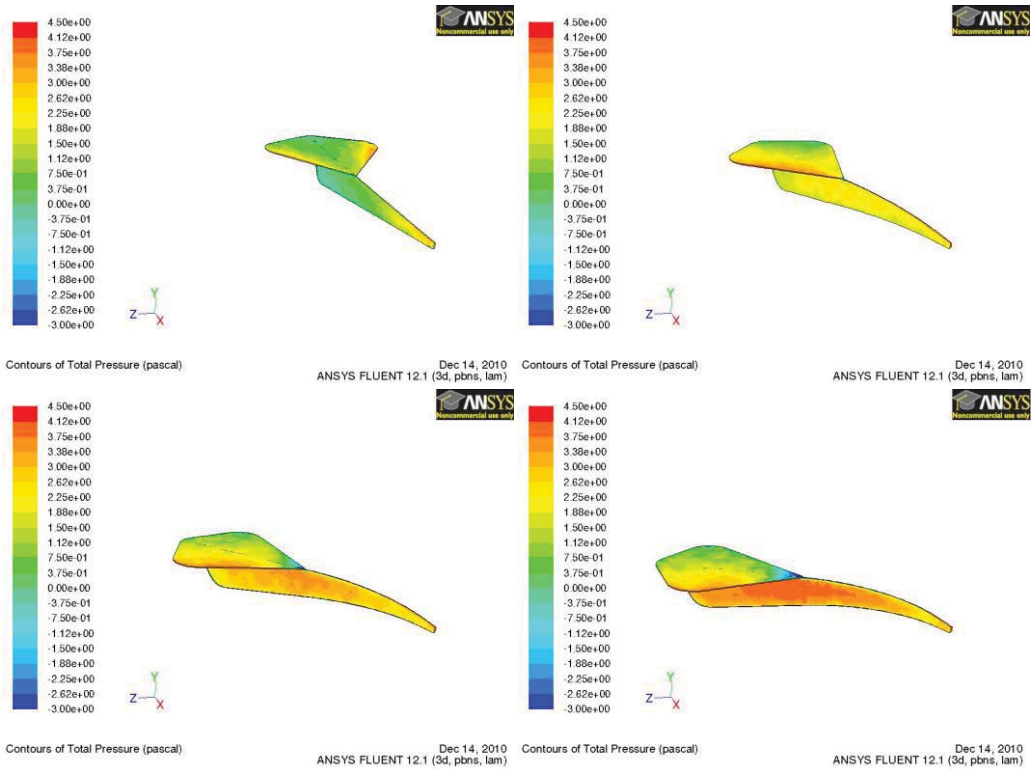

Figure 14. Pressure Distribution of Tail 1 α_t = -10°. *0 degree tail flex (top left), 20 degree tail flex (top right), 40 degree tail flex (bottom left), 60 degree tail flex (bottom right).*

Table 4. Computational Fluid Dynamics Results for α_t = -10°.

Tail Deflection Angle	*Drag (10^{-6} N)*	*Lift (10^{-6} N)*	*Momentum (10^{-6} Nm)*		
			X - axis	*Y - axis*	*Z - axis*
0°	-64.48	-663.00	-0.26	-0.34	112.97
20°	-356.00	-792.90	24.04	-101.45	133.69
40°	-1168.00	-215.90	12.83	-212.66	41.83
60°	-2101.10	231.63	-0.33	-255.95	-46.71

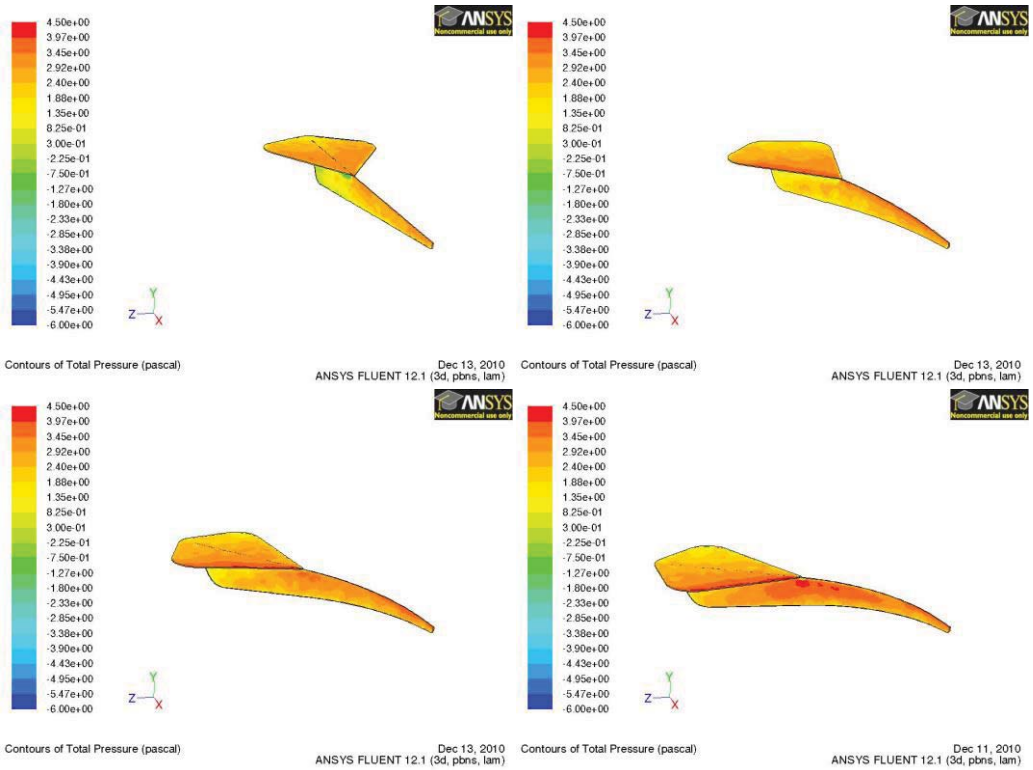

Figure 15. Pressure Distribution of Tail 2 α_t = -30° . *0 degree tail flex (top left), 20 degree tail flex (top right), 40 degree tail flex (bottom left), 60 degree tail flex (bottom right).*

Table 5. Computational Fluid Dynamics Results for α_t = -30°.

Tail Deflection Angle	*Drag (10^{-6} N)*	*Lift (10^{-6} N)*	*Momentum (10^{-6} Nm)*		
			X - axis	*Y - axis*	*Z - axis*
0°	-73.34	-2755.00	-0.26	-0.89	468.60
20°	-323.98	-3183.30	103.21	-95.89	525.47
40°	-900.81	-2692.96	165.19	-160.00	405.03
60°	-1575.20	-2272.30	201.26	-185.59	267.46

G. Discussion

Observations describing the flight characteristics of tail 1 and tail 2 were made from the trajectory analysis results and pilot feedback. The CG calculations and CFD analysis provided a basis for explaining the flight characteristics observed. Although tail 2 outperformed tail 1 in agility, the pilot observed that tail 1 permitted more stable flight speeds. Results from the trajectory analysis revealed that tail 1 provided a more uniform velocity magnitude during turns (This can be seen by comparing the variation of the velocity magnitudes for each tail in Fig. 14 and Fig. 15). The drag and lift forces acting on tail 1 generated significantly lower pitch moments than on tail 2. The reduction in pitch moment would have reduced λ to yield a stronger thrust component. It was also observed that tail 1 performed more mild banked turns. CFD results indicate that lateral deflections of tail 1 contributed greater yaw influence and lesser roll influence than tail 2. The roll moments derived for tail 2 exceeded the yawing moments, which may have explained its steeper banked-turn behavior.

Both tails behaved similarly under extreme tail deflection. At 60° flexure the vehicle had a tendency to bank steeply and spiral downward. The most functional range of flexure for both tails was examined to be between 0° and 40°. Mild deflections accomplished more stable turns with lesser roll motion. Tables 4 and 5 of the CFD analysis accounted for this by illustrating that tail curvatures exceeding 40° resulted in significant pitch moment decline. Weaker pitch moments would result in less lift generated. Therefore, the pilot concluded that adequate control authority and stability was achieved with tail deflections within the 40° range.

IV. Summary

Utilizing a flexible tail mechanism to mimic abdominal deflection of insects has shown to be a capable method of control for a flapping wing MAV. The experimental vehicle demonstrated the use of lateral tail deflections to propagate aerodynamic and gravitational torques effectively. The investigative results of the trajectory analysis, CG displacement analysis, and CFD analysis verified that the tail provides enough control authority to maneuver the vehicle directionally and laterally. Therefore, pairing both body and wing kinematics to achieve maneuverability in future flapping wing MAV's has the potential to be very useful. Tail deflection could be useful not only for achieving advanced maneuverability but also stabilizing the vehicle when encountering environmental disturbances such as wind gusts. Mimicking abdominal deflections of insects contributes greatly in achieving the "hide in plain sight" mission objective. By replacing rigid body joints and control flaps with compliant mechanisms the vehicle can be made more difficult to distinguish from nature, especially with future development of piezo electrics and artificial muscle fibers (smart materials). Applying the use of tail deflection in conjunction with wing kinematics has the potential to spawn a new breed of bio-inspired micro air vehicles.

Future efforts will be made in expanding the current research base on bio-inspired flight control mechanisms. The methodologies outlined in this work will aide in the exploration of newer components and control surfaces that better reflect those mechanisms found in nature. Other tools will be used to push the data collection from a medium fidelity to a high fidelity approach such as particle image velocimetry (PIV) in a wind tunnel and more resolved models for CFD such as flow-structure interaction models that actively deform under aerodynamic loading according to real-world material properties. These future works will serve as a basis on finding an optimum control system for flapping wing MAVs that provides agile, yet stable, flight characteristics while resembling creatures found in nature.

Acknowledgments

The authors would like to thank Dr. George Huang and his students at WSU for the generous use of their lab equipment as well as the previous Senior Capstone design teams who have worked on similar MAV topics for their suggestions and wisdom on the subject. A special thanks is given to Dr. Greg Parker and the AFRL for their funding contributions. Lastly, the authors would like to thank Dr. Joseph Shang for his generous donation to support the presentation of the paper.

References

[1]Taylor, T.K. "Mechanics and Aerodynamics of Insect Flight Control," Biol. Rev.76:449-471, 2001

[2]Dudley, R. *The Biomechanics of Insect Flight*, Princeton University Press, Princeton, New Jersey 2000, Chaps. 3-5.

[3]Dudley, R. "Mechanisms and Implications of Animal Flight Maneuverability" Integ and Comp. Biol 42:135-140, 2002.

[4]Ellington, C.P. "The Novel Aerodynamics of Insect Flight: Applications to Micro Air Vehicles" J. Exp. Biol. 202:3439-3448, 1999.

[5]Zanker, J.M. "How Does Lateral Abdomen Deflection Contribute to Flight Control of Drosophila Melanogaster?" J,Comp. Physiol. A 162:581-688, 1988.

[6] Lorez M. "Neural Control of Hindleg Steering in Flight in the Locust" J. Exp. Biol. 198:869-875, 1995.

[7]Gotz K.G., Hengstenberg,B., and Biseinger,R.(1979). "Optomotor Control of Wing Beat and Body Posture in Drosophila" Biol. Cybern. 35:101-112.

[8]Camhi, J.M. "Sensory Control of Abdomen Posture in Flying Locusts" J. Exp.biol. 52: 533-537, 1970.

[9]Wagner H. "Flight Performance and Visual Control of Flight of the Free Flying Housefly (Musca domestica L.)I. Organization of Flight Motor." Phil. Trans. R. Soc. Lond. B 312:553-579, 1986.

[10]Zanker, J.M. "On the Mechanism of Speed and Altitude Control in Drosophila Melanogaster" Physiol Entomol. 13, 1988.

[11]de Croon G.C.H.E., de Clerq, K.M.E., Ruisjsink, R., Remes B.. and de Wagter, C. "Design, Aerodynamics and Visionbased Control of the Delfly" Int. J. MAV. Vol. 1, Num. 2 :71-79, 2009.

[12]Pornsin-Sirirak, T.N., Tai, Y.C., Ho, C.H. and Keenon, M, "Microbat: A Palm-sized Electrically Powered Ornithopter." NASA/JPL Workshop on Biomorphic Robotics, Pasadena, California 2001.

[13]Stanford, B., Abdulrahim, M., Lind, R., Ifju, P. "Design and Optimization of Morphing Mechanisms for Highly Flexible Micro Air Vehicles," *AIAA Structures, Structural Dynamics, and Materials Conference*, AIAA, Newport, Rhode Island, 2006.

[14]Johnson, B., Claxton, D., Stanford, B., Jagdale, V., Ifju, P. "Development of a Composite Bendable-Wing Micro Air Vehicle," *45th AIAA Aerospace Meeting and Exhibit*, Reno, Nevada, 2007.

[15]Ifju, P., Stanford, B., Sytsma, M., "Analysis of a Flexible Wing Micro Air Vehicle," *25th AIAA Aerodynamic Measurement Technology and Ground Testing Conference*, San Fanscisco, California, 2006.

[16]Ifju, P. J., Ettinger, S., Jenkins, D. Martinez, L. " Composite Materials for Micro Air Vehicles," University of Florida, 2000.

[17]Boller, C., Kuo, C., Qin, N. "Aproaching Morphing Wing Concepts on the Basis of Micro Aerial Vehicles," Proc. of SPIE Vol. 6521, 65270K, 2007.

[18] Dong, H. Koehler, C. Liang, Z. Wan, H., and Gaston, Z. "An Integrated Analysis of a Dragonfly in Free Flight," *40th AIAA Fluid Dynamics Conference and Exhibit*, 2010-4390, 2010.